Sensors and Actuators A 313 (2020) 112198

Contents lists available at ScienceDirect

Sensors and Actuators A: Physical

journal homepage: www.elsevier.com/locate/sna

A low-profile flexural displacement-converter mechanism for piezoelectric stack actuators

F. Tajdari[a,*], A.P. Berkhoff[a,b], M. Naves[a], M. Nijenhuis[a], A. de Boer[a]

[a] University of Twente, Faculty of Engineering Technology, Drienerlolaan 5, 7500 AE Enschede, The Netherlands
[b] TNO Technical Sciences, Acoustics and Sonar, Oude Waalsdorperweg 63, 2597AK Den Haag, The Netherlands

ARTICLE INFO

Article history:
Received 20 October 2019
Received in revised form 5 June 2020
Accepted 6 July 2020
Available online 17 July 2020

Keywords:
Thin
Flexure-based mechanism
Motion-converter
Piezoelectric stack actuators
Pure translation

ABSTRACT

A thin flexure-based mechanism is proposed that is useful in applications with limited build space. The proposed mechanism converts the initial in-plane motion of two piezoelectric stack actuators to an out-of-plane translational motion. Two actuators in the symmetric design of the proposed APA can be used to ensure a pure translation output motion. A Finite Element (FE) model is used to analyze the rigid multibody model of the proposed mechanism. The rigid multibody model is used to design the desired flexural mechanism in a three-dimensional space. The proposed design is then manufactured and is subjected to an experimental study. Measurements validate the performance of the proposed design with an error of less than 15%. A parametric study on the effect of the applied voltage to the actuators of the proposed mechanism reveals good agreement between the numerical model and the manufactured mechanism.

1. Introduction

Piezoelectric stack actuators can be conveniently used in applications where a high structural force is needed [1]. These actuators can provide a driving force as high as two kilonewtons to a mechanical structure [2]. Piezoelectric stack elements are linear actuators that can undergo large compressive loads before reaching their blocked force [2]. However, they cannot bear tensile forces [3]. The total displacement of piezoelectric stack elements is the summation of the displacement of each individual layer [3]. Therefore, a longer actuator has a larger output displacement. In practice, multiple layers of piezoelectric elements are mounted on top of each other to achieve a large output displacement [3]. These stacked layers are typically mechanically in series and electrically in parallel [3]. Piezo-stepper motors consist of multiple piezoelectric actuators that both expand and bend sideways. Although each pair of actuators moves just a few microns per cycle, piezo-stepper motors can allow for very long travel lengths at high speeds. However, large disturbances and vibrations are inevitable in the operation of piezo-steppers. Therefore, control schemes are needed to reduce the unwanted disturbances [4]. High operating frequency and large thickness make the piezo-steppers inappropriate for low frequency applications with limited build space.

In applications with limited build space, the placement of piezoelectric stack actuators may be restricted by the surrounding mechanical parts. A limited build space does not allow for the application of relatively large piezoelectric stack actuators. However, a large piezoelectric element is required when a large structural displacement is desired [3]. In particular, one practical application for piezoelectric stack actuators in the low frequency range (from 20 Hz to 500 Hz) would be in the excitation part of a thin acoustic source. An optimization study in earlier research revealed that a long piezoelectric stack actuator with a length of approximately 73 mm was needed to obtain the maximum acoustical radiated power [5]. The optimum piezoelectric actuator can provide a combination of both a displacement and a force to the connected acoustic source with magnitudes of respectively 14 μm and 100 N. However, the limited build space of the thin acoustic source does not allow for a direct use of the piezoelectric device.

In this paper, a thin actuation mechanism is referred to as a mechanism with a size ratio less than 2. The size ratio is defined as the ratio between the size of the mechanism in the direction of the final motion and the thickness of the piezoelectric actuators. This thin actuation mechanism can be employed in the thin acoustic source that is shown in Fig. 1. The required actuation mechanism should fit in the limited build space of the air gap of the acoustic source. A maximum height of approximately 10.5 mm in the direction of the final motion is needed for the actuation mechanism to

* Corresponding author.
E-mail addresses: f.tajdari@alumnus.utwente.nl (F. Tajdari), a.p.berkhoff@utwente.nl (A.P. Berkhoff), m.naves@utwente.nl (M. Naves), m.nijenhuis@utwente.nl (M. Nijenhuis), a.deboer@utwente.nl (A. de Boer).

https://doi.org/10.1016/j.sna.2020.112198
0924-4247/

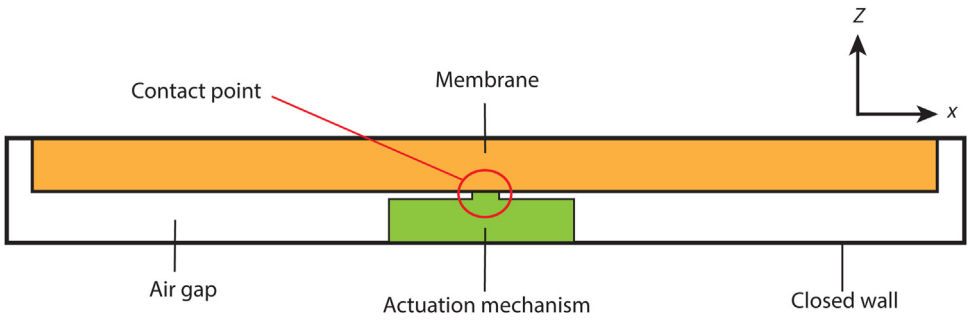

Fig. 1. Application of the required flexural mechanism as the actuation unit of a thin acoustic source.

Table 1
A comparison among various designs.

Design	Fig.	Conversion	pure translation	Resonance > 1000 Hz	Ratio
Lever	2 (a)	√	×	–	1.1 √
Energy harvester	2 (b)	√	√	–	3 ×
3D bridge	2 (c)	√	×	×	5 ×
3D rhombic	2 (d)	√	√	√	3 ×
Honeycomb	2 (e)	√	√	×	1.1 √
In-plane	2 (f)	×	√	√	2 √
2D bridge	2 (g)	√	√	×	3 ×
2D rhombic	2 (h)	√	√	–	7 ×
Proposed design	3 (b)	√	√	√	1.9 √

fit in the air gap in this application [5]. This height requirement is defined relative to the large surface area of the thin acoustic source membrane, which is in the size of a standard A4 paper and has a mass of approximately 175 g [5]. This required height is considered thin for the actuation mechanism relative to the size of the acoustic source [5]. The required actuation mechanism has to be sufficiently thin and should be able to deliver a force of 100 N and a displacement of 14 μm needed by the thin acoustic source. The coupled acoustic source system, including the actuation mechanism, should have a pure translation motion in the frequency range between 20 Hz and 500 Hz. A fundamental resonance peak at frequencies higher than 1000 Hz for the actuation mechanism ensures this pure translation motion for the coupled acoustic source system below 500 Hz.

One option to employ large piezoelectric devices in applications with limited build space in the direction of motion, is to use auxiliary mechanical structures. The auxiliary structure can be used in combination with the piezoelectric elements as a motion-converter mechanism, and can be fitted in a space with a limited dimension. The motion of the long piezoelectric actuators can be converted into another direction of motion using the motion-converter mechanism. Flexures may be used in the design of the auxiliary mechanical structure. Flexures are elastically deforming parts that provide repeatable motion in the desired degrees of freedom [6,7]. Due to the absence of friction, backlash and wear, the mechanism generates predictable and maintenance-free motion with low hysteresis.

Amplified piezoelectric actuators (APAs) are piezoelectric actuators integrated with flexure-based mechanisms to either amplify the displacement of the actuators or to change their direction of motion. In this research, a flexural mechanism is desired to change the direction of motion of the actuators. The desired flexural mechanism in the current study has to have a sufficiently small dimension in the final direction of motion with the limited build space. A dimension as small as approximately 10.5 mm is considered in this work. The small dimension has to be comparable to the thickness of the piezoelectric actuators. Piezoelectric stack devices with a thickness up to 6 mm are required in this research to be employed in the limited build space. The fundamental resonance frequency of the desired mechanism has to be higher than 1000 Hz. This ensures that the fundamental resonance of the desired mechanism is not within the resonance frequency of the connected mechanical structure. An output displacement that is approximately equal to the displacement of the actuators (approximately 14 μm) is sufficient in this work. Therefore, the suggested flexural mechanism in this research is a motion-converter mechanism, and the amplification of the motion is not an initial design factor. A higher amplification ratio between the input and output motions results in using smaller piezoelectric actuators, and leads to a more cost-efficient design. However, in this research, the main focus is on the conversion of the direction of motion to keep the output displacement and force close to the input values. Therefore, an output force that is approximately equal to the applied force by the actuators is required in the final design (approximately 100 N).

In the majority of the proposed APA designs, the spatial constraint is not of high importance while the high amplification ratio is [8,9]. Using amplifying mechanisms in flexural designs is an approach to increase either the output force or the resulting displacement of piezoelectric elements [8]. APAs are useful in optical applications, nano- and micro-scale positioning [10–13], vibration isolation [14], and energy harvesting [15,16]. Depending on the required amplification ratio and the desired degrees of freedom, various mechanisms have been designed. Some available APA designs are shown in Fig. 2. Various designs are compared in Table 1 in terms of their ability to convert the direction of motion, the possibility of a pure translation output motion, the resonance frequency (desired range above 1000 Hz) and their size ratio in the direction of the output motion. In this paper, a size ratio less than 2 is required. A lever is a known mechanism that is used to translate the displacement of piezoelectric actuators [14]. However, due to a parasitic rotational motion, a pure vertical displacement is not achieved (see Fig. 2(a)). The mechanism shown in Fig. 2(b) is used as an energy-harvester that converts a pure translation motion to a piezoelectric device [16]. However, the suggested energy harvester is not thin compared with the thickness of the piezoelectric device. Although the mechanism shown in Fig. 2(c) reaches an amplification ratio as high as 10, the existence of a parasitic motion is inevitable [17]. If a parasitic motion is present, the output motion is not a pure trans-

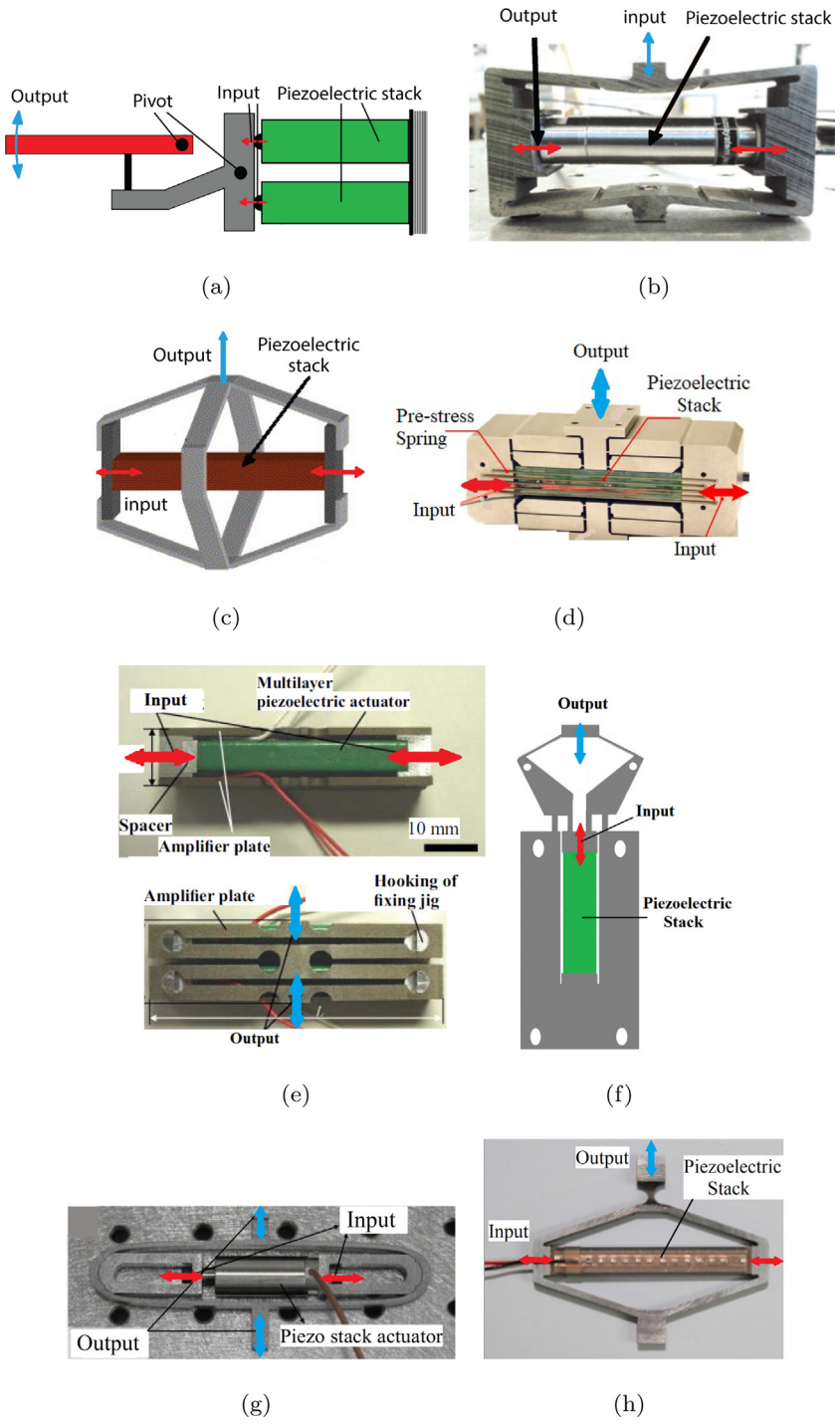

Fig. 2. Available designs of amplified piezoelectric actuators: (a) lever [14]; (b) energy-harvester [16]; (c) 3D bridge [17]; (d) 3D rhombic [18]; (e) honeycomb [19]; (f) in-plane [20]; (g) 2D bridge [21]; (h) 2D rhombic [22].

lation. A symmetric displacement-converter mechanism is shown in Fig. 2(d) [18]. This mechanism has a pure translation output displacement. The fundamental resonance frequency of this design is above 1000 Hz. On the other hand, the dimension in the direction of the final motion is as large as approximately three times the thickness of the piezoelectric actuator. In another design, a "honeycomb" mechanism is proposed that can generate an output displacement that is up to 7 times larger than the displacement of the piezoelectric actuator [19]. However, this mechanism has a resonance at 400 Hz (see Fig. 2(e)). The mechanism shown in Fig. 2(f), has a resonance frequency above 1000 Hz [20]. However, the output motion is in the same direction as the input. The suggested flexural mechanisms shown in Figs. 2(g) [21] and 2 (h) [22], are not thin relative to the thickness of the piezoelectric actuators. Therefore, they cannot be used in applications with limited build space. According to Table 1, the designs shown in Fig. 2 are either not suitable for applications at low frequencies (due to the existence of a resonance frequency in the low frequency range below 1000 Hz), or they are unable to deliver the required force or displacement that is required in this research (100 N force and 14 μm displacement). Although a larger scale of the designs shown in Fig. 2(b), (d), (g) and (h) may provide the required force or displacement in the present

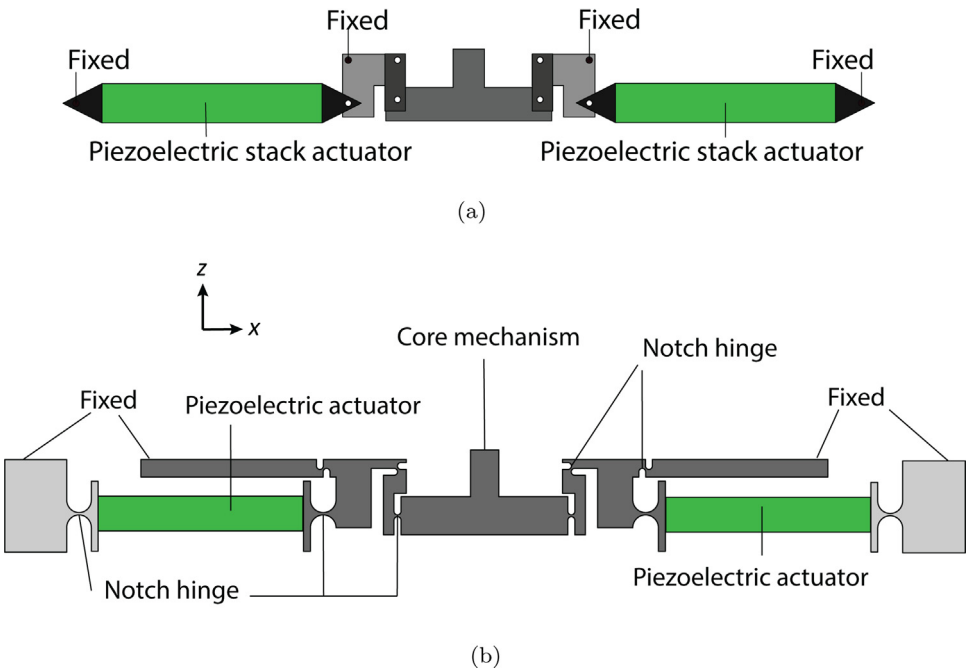

Fig. 3. The suggested motion-converter mechanism: (a) the rigid multibody dynamics mechanism; (b) the complete assembly of the flexural mechanism.

work, they are not fitted in the small build space of 10.5 mm in this study. However, the kinematic principles used in these designs can be developed to propose an appropriate flexural motion-converter mechanism.

Available commercial APAs are easy to manufacture, and can be produced in a wide range of output displacements (see Refs. [23,24]). However, due to the fact that they are produced with specific dimensions and fixed aspect ratios, they are either not suitable for applications with limited build space, or they cannot provide the required output force in this research.

In the present paper, a flexure-based mechanism is proposed. The suggested mechanism is thinner than the available designs. It measures only 10.5 mm in the desired direction of motion. Therefore, it can be employed for applications with spatial constraints. The proposed compliant model aims at translating an in-plane displacement of two piezoelectric stack actuators to an out-of-plane motion perpendicular to the reference plane. Two actuators in the symmetric design of the proposed APA can be used to ensure a pure translation output motion without the presence of any parasitic motion. The fundamental resonance frequency of the suggested mechanism occurs at frequencies above 1000 Hz. This high resonance frequency ensures that in the frequency range of interest in the current study (frequencies between 20 Hz and 1000 Hz) no modes of the connected mechanical structure are excited. Therefore, the proposed motion-converter mechanism in this research can be used in applications with limited build space, when a pistonic motion is required.

In this research, design principles of the proposed flexural motion-converter mechanism are described. A numerical Finite Element (FE) model is used to analyze a multibody model of the proposed design, which consists of rigid bodies and hinge joints. The relative rotation of the joints, the applied forces to the joints, and the stress distribution in the linkages of the motion-converter mechanism are analyzed in the multibody model. A flexure-based mechanism is designed using the result of this multibody analysis. A FE model of the flexural mechanism is analyzed to obtain the output motion of the suggested motion-converter mechanism. A prototype of the proposed design is manufactured, and an experimental study is provided to validate the suggested thin design. A parametric FE study investigates the effect of the applied electrical voltage to the actuators on the output motion of the proposed flexural mechanism.

2. Design approach

The proposed thin motion-converter mechanism is schematically shown in Fig. 3. The deflected motion-converter mechanism will be shown in Fig. 11, and the numerical analysis will be described in more details in Section 3. A rigid multibody model of the motion-converter mechanism is shown in Fig. 3(a), which will be used in Section 3.1 to design the required dimensions of the motion-converter mechanism. The rigid multibody model in Fig. 3(a) has four fixed hinge joints, and can be converted to a flexure-based counterpart in Fig. 3(b). The core part of the suggested flexural mechanism is a monolithic mechanism, and is shown in Fig. 4. The reason for designing the proposed mechanism in a single piece is to make it friction-free without any external connections. Two piezoelectric stack actuators are mounted in the xy-plane and along the x-axis. Using two actuators can ensure that the output motion is a pure translation. The two piezoelectric actuators are fixed on one side using flexural notch hinges. The actuators apply axial loads to linkage 1 and linkage 7 in the direction of the x-axis (see Fig. 4(b)). The mechanism is connected to the fixed world through linkages 8. The applied loads rotate linkage 2 counter-clockwise and linkage 6 clockwise around the fixed centers of rotations j_2 and j_7, respectively. The two mirrored rotations trigger linkage 3 and linkage 5 to move vertically in the positive direction of the z-axis. The upward motion of linkage 3 and linkage 5 pulls linkage 4 upward. The pure vertical motion of linkage 4 is achieved thanks to the symmetric design of the flexural mechanism. This upward motion of linkage 4 is the output displacement of the motion-translator.

The suggested design has a depth of 21.5 mm in the direction of the y-axis. It is sufficiently stiff in that direction, therefore, no parasitic motion is present. Due to using two piezoelectric actuators in a symmetric design, no parasitic motion is present in the direction of the x-axis. Therefore, the only possible motion is in the direction of the z-axis. The dimensions of the proposed flexural

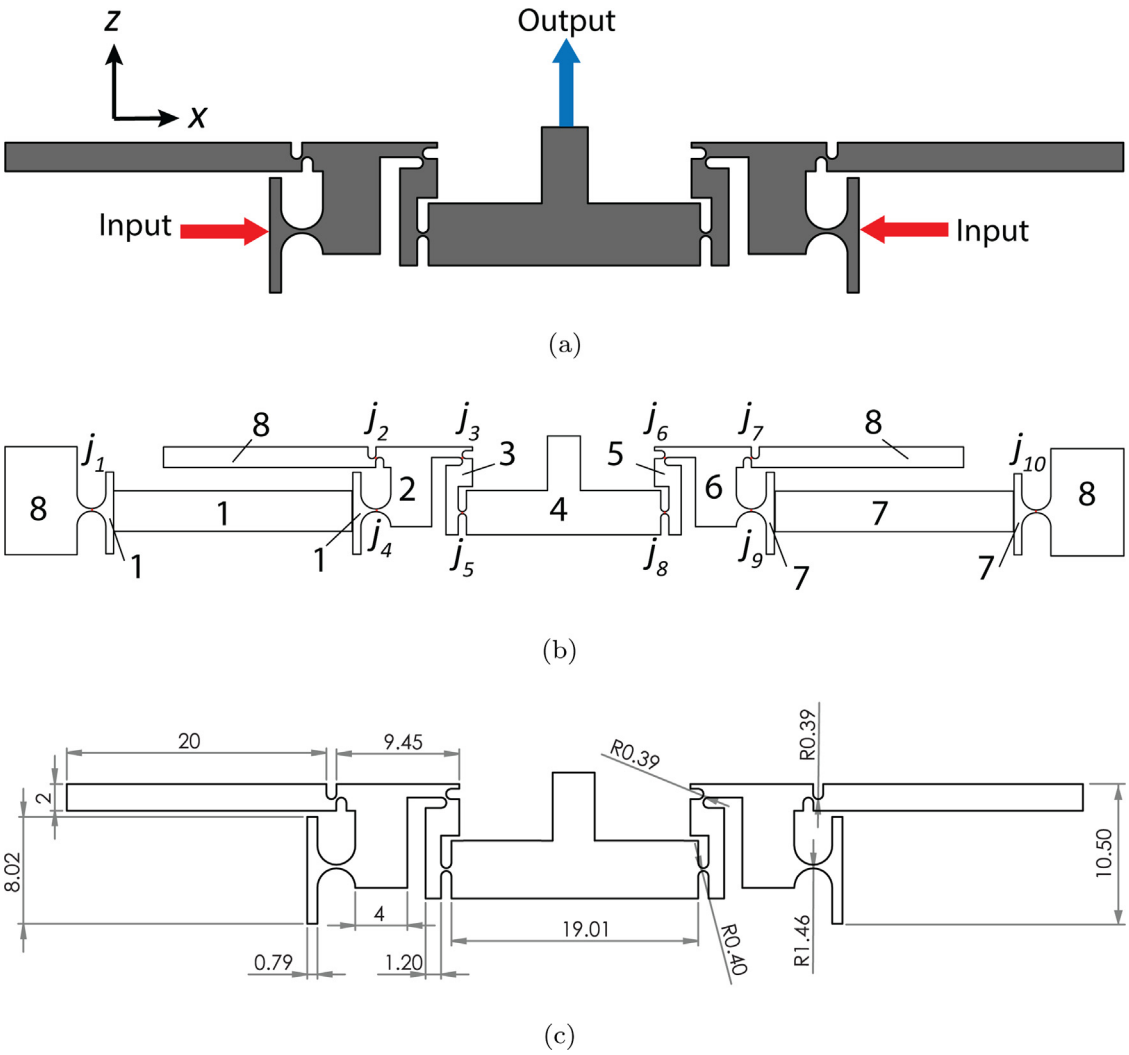

Fig. 4. The monolithic core part of the suggested flexure-based mechanism: (a) the input and output directions of motion in the mechanism; (b) linkages and joints of the mechanism for the case of locked actuators; (c) dimensions of the mechanism in millimeter.

mechanism are shown in Fig. 4(c). The dimension of the mechanism in the direction of motion is 10.5 mm. This dimension is relatively small compared to the dimension of the mechanism in the direction of the *x*-axis (77 mm). It has to be mentioned that no parasitic motion occurs if both actuators displace the same amount. However, in practice, similar displacement of the two actuators cannot be fully achieved. This is due to the small tolerance that occurs during the manufacturing process of the actuators.

2.1. Design requirements and considerations

An important design parameter in this research is the dimension of the displacement-converter mechanism in the direction of the output motion (*z*-axis). The proposed motion-converter mechanism is designed in such a way that its dimension in the direction of the *z*-axis is considerably smaller than that in the direction of the *x*-axis.

The 3D geometry of the proposed mechanism can be easily projected into the *xz*-plane. Therefore, the suggested mechanism is easily manufacturable using structural steel and the wire EDM (Electrical Discharge Machining) technique [25].

Another important factor is the number of degrees of freedom (DOF). According to Fig. 4(b), the flexural mechanism is a seven-bar linkage. Considering the ground as a single linkage and the length of

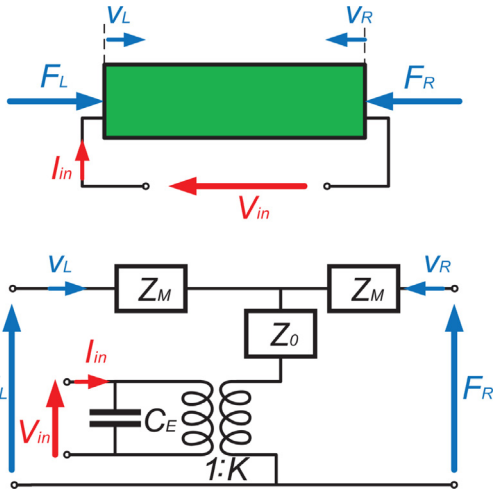

Fig. 5. A three-port equivalent electrical circuit of piezoelectric stack actuators.

the actuators locked, there are a total of 8 linkages in the mechanism ($N = 8$). Furthermore, the mechanism contains 10 hinge joints as connections between the linkages (j_1 to j_{10} in Fig. 4(b)). Therefore, the number of single-DOF joints, m, is 10 in total. Using Grübler's

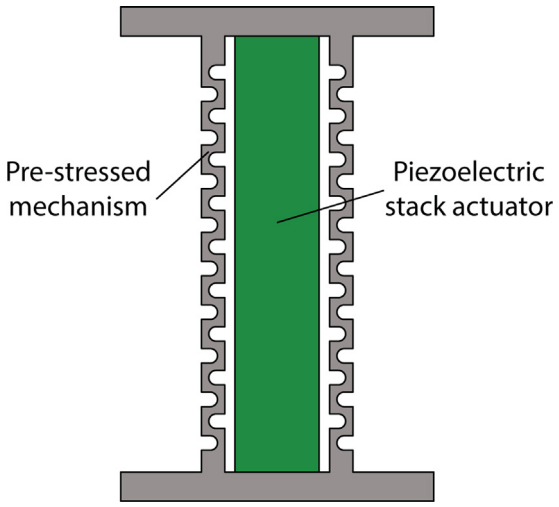

Fig. 6. Pre-stressing mechanism that uses similar design as the suggested design by Cedrat Technologies [30].

formula [7], and considering locked actuators, one can determine the planar degrees of freedom of the kinematic chain as:

$$DOF = 3N - 2m - 3 = 1. \tag{1}$$

According to Eq. (1), the mechanism has only one planar degree of freedom in the case of locked actuators. For the application in a thin acoustic source, the membrane stiffness of the acoustic source imposes an additional constraint to the proposed mechanism in the lateral x-direction (see Fig. 1). This membrane stiffness provides a constraint in the x-direction and can eliminate the remaining degree of freedom. For the application in the thin acoustic source, the proposed mechanism has a pure translation output motion in the direction of the z-axis. The mechanism is designed in 3D space such that the two translations in the direction of the x- and the y-axis are constrained. In addition, due to symmetry, all three rotational degrees of freedom have to be constrained. Therefore, the proposed design has a pure vertical translation in the direction of the z-axis. Using two actuators in a symmetric mechanism can ensure this pure translation output motion.

2.2. Piezoelectric stack actuators

Multilayer piezoelectric actuators are commonly modeled using either constitutive equations [26], or equivalent electrical circuits [27]. In the current study, a three-port equivalent electrical circuit, which is introduced in [28], is rearranged to model linear piezoelectric devices. The proposed equivalent electrical circuit in Ref. [28] is shown in Fig. 5. The equivalent circuit is called the three-port circuit since there are in total three external terminals. One port accounts for the applied electrical voltage and the resulting current, and two ports take the external mechanical forces into account. Let F_R and F_L be the applied structural forces to the piezoelectric actuator through the right and left boundaries, respectively; then v_R and v_L are the velocity of the right and left boundaries of the piezoelectric device, respectively. V_{in} and I_{in} are the applied electrical voltage and current to the piezoelectric actuator, respectively.

According to Fig. 5, the parameter C_E is the electrical capacitance of the piezoelectric actuator, which can be formulated as:

$$C_E = \frac{n\acute{\epsilon}A}{l}, \tag{2}$$

where l, A, and n are the total length, surface area, and the number of stacked layers of the piezoelectric device, respectively, and $\acute{\epsilon}$ is defined as:

$$\acute{\epsilon} = n^2\epsilon^T - \frac{(nd_{33})^2}{s^E}, \tag{3}$$

in which ϵ^T, d_{33} and s^E are dielectric permittivity at constant stress, piezoelectric constant and elastic compliance at constant electric field, respectively. One can derive the mechanical impedances of the piezoelectric device, Z_0 and Z_M, using the following two equations:

$$Z_0 = \frac{\acute{c}aA}{j\omega \sin(al)}, \tag{4}$$

$$Z_M = Z_0(\cos(al) - 1), \tag{5}$$

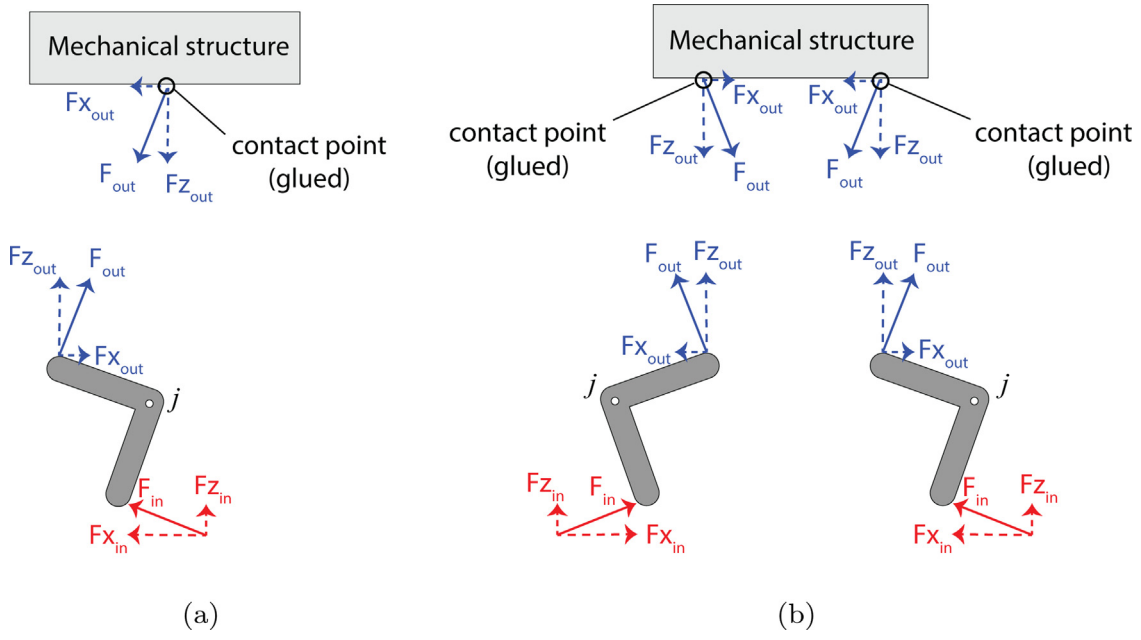

Fig. 7. Elbow-lever motion-converters: (a) single; (b) double.

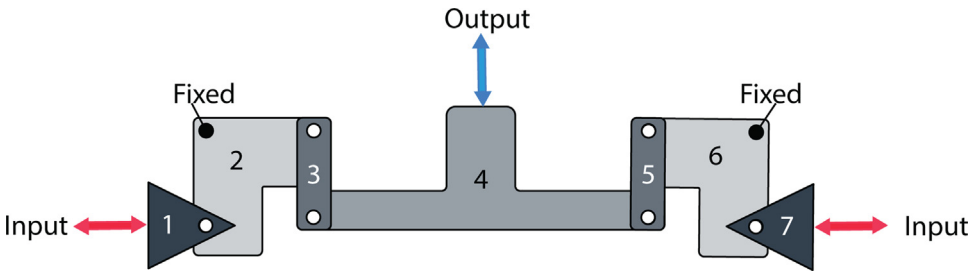

Fig. 8. Rigid multibody model of the suggested mechanism.

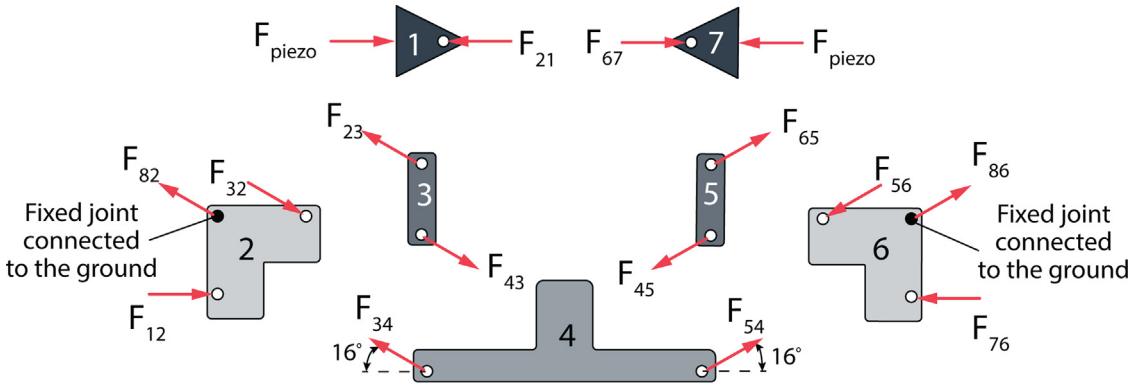

Fig. 9. Free body diagram of the rigid multibody mechanism.

where ω is the angular frequency. Parameters $\hat{c}$, $\hat{\epsilon}$ and $\hat{e}$ are piezoelectric coefficients and can be defined as:

$$\hat{c} = \frac{1}{s^E}, \tag{6}$$

$$\hat{e} = \frac{nd_{33}}{s^E}. \tag{7}$$

The parameter a in Eqs. (4) and (5) can be defined as:

$$a = \sqrt{\rho s^E}, \tag{8}$$

where ρ denotes the density of the piezoelectric device. The conversion coefficient, K, is formulated as:

$$K = \frac{A\hat{e}}{l}. \tag{9}$$

K is the conversion ratio between the electrical and the mechanical domains. According to Eqs. (2) to (9), the three-port equivalent circuit can be written in matrix form as:

$$\begin{bmatrix} F_R \\ F_L \\ V_{in} \end{bmatrix} = \begin{bmatrix} -(Z_M + Z_0 + \frac{K^2}{C_E j\omega}) & Z_0 + \frac{K^2}{C_E j\omega} & \frac{K}{C_E j\omega} \\ -(Z_0 + \frac{K^2}{C_E j\omega}) & Z_M + Z_0 + \frac{K^2}{C_E j\omega} & \frac{K}{C_E j\omega} \\ -\frac{K}{C_E j\omega} & \frac{K}{C_E j\omega} & \frac{1}{C_E j\omega} \end{bmatrix} \begin{bmatrix} v_R \\ v_L \\ I_{in} \end{bmatrix}. \tag{10}$$

Using either the equivalent electrical circuit shown in Fig. 5, or the equivalent equations in matrix form shown in Eq. (10), one can determine the applied forces to the piezoelectric multilayer actuator. For a comprehensive explanation on the derived expressions see Ref. [28].

2.3. Pre-stressing mechanism

As mentioned earlier, piezoelectric stack devices cannot bear tensile forces. With the aid of a pre-stressing mechanism, tensile forces are avoided during the dynamic operation of the actuator. It is recommended to have approximately 10 MPa to 20 MPa as an initial compression [29]. Commercial pre-stressing mechanisms are produced as integrated pre-stressed piezoelectric devices [30]. Therefore, a single pre-stressing mechanism is not available as a separate unit. In the present work, a compliant mechanism is designed in accordance with the design principles used by Cedrat Technologies [30]. The designed mechanism applies a pre-stress of 4 MPa to the piezoelectric stack actuator. Although the applied pre-stress is not within the recommended range, it is sufficient in the current study. The reason is that the applied voltage to the piezoelectric actuators in the experiment is low and remains between zero and a positive value, and therefore, no tensile force is present. The pre-stressing mechanism is schematically shown in Fig. 6. As seen in the figure, the pre-stressing mechanism resembles a spring that is mounted in parallel with the piezoelectric stack actuator. Since the pre-stressing mechanism is initially shorter than the piezoelectric element, a tensile stress of approximately 4 MPa is needed to fit the piezoelectric actuator in place. The pre-stressing mechanism is made of high strength steel. The required expansion of the pre-stressing mechanism to fit the piezoelectric actuator is approximately 0.2 mm. A load of approximately 300 N is needed to deform the pre-stressing mechanism. The stiffness of the pre-stressing mechanism is approximately 1.5 N/μm, which is much less than the stiffness of the piezoelectric stack actuators (43 N/μm, [31]). Therefore, the stiffness of the piezoelectric stack actuator remains the dominant stiffness in the combined pre-stressing mechanism. A tensile pre-stress of approximately 8.3 MPa is applied to the pre-stressing mechanism to deform 0.2 mm. This tensile stress does not exceed the yield stress of 1500 MPa of high strength steel. Fatigue is not present because the maximum stress in the pre-stressing mechanisms is sufficiently lower than 50% of the yield stress of the material. This low stress prevents fatigue and ensures that the pre-stressing mechanism lasts for more than 10^8 life-cycles).

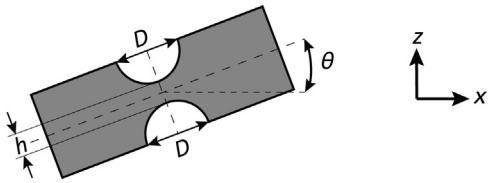

Fig. 10. A flexural notch hinge.

2.4. Design procedures

As mentioned earlier, the proposed compliant mechanism has a pure translation in the direction of the *z*-axis. Due to the limited build space in the direction of the *z*-axis, a lever-like mechanism can be useful. An elbow-lever mechanism is suitable for changing the direction of motion. As shown in Fig. 7(a), the elbow-lever pivots the horizontal deformation of the actuator 90 degrees on the final vertical direction. However, the rotary motion of the elbow-lever causes an unwanted parasitic motion of the output stage in the direction of the *x*-axis. One contact point between the single elbow-lever and the connected mechanical structure is present. Therefore, using a single elbow-lever is not sufficient in the design of the motion-converter mechanism.

Using two actuators in a symmetric design with two elbow-levers can eliminate the final parasitic motion. According to Fig. 7(b), two symmetric 90-degree elbow-levers can be used to produce a pure vertical motion. Using two mirrored elbow-levers results in two contact points between the levers and the connected mechanical structure. Since the elbow-levers are ideally glued to the external mechanical structure, no relative rotation exists in the contact points. Although using two symmetric elbow-levers eliminates the parasitic motions in the direction of the *x*-axis, horizontal shear loads and moments are applied to the connected mechanical structure through the glued contact points. As a result of the applied moment, the mechanical structure undergoes bending. A single contact point is desired to eliminate the transmission of the moments to the external mechanical structure and ensure an accurate output with no parasitic motion. In this work, a design is proposed that suggests a single contact point as the connection between the elbow-lever and the mechanical structure. Using two actuators in the symmetric design proposed in this study can translate two horizontal input motions to a pure translation vertical output motion.

2.4.1. Rigid multibody model

Rigid linkages are used in a preliminary model of the suggested mechanism. According to Eq. (1) and Fig. 4(b), the proposed mechanism is a seven-bar linkage. Considering each linkage as a rigid bar, a rigid multibody counterpart of the proposed flexure-based model is obtained and is shown in Fig. 8. As seen in the figure, two fixed hinge joints are used as the connection points of the rigid linkages to the ground (see linkages 2 and 6 in Fig. 8). A free body diagram of each part of the rigid mechanism is shown in Fig. 9. The applied forces to linkage 4 have an angle of 16° with respect to the *x*-axis.

2.4.2. Flexural model

The rigid multibody model of the suggested mechanism is useful in designing its flexural counterpart. The amplitude and the direction of reaction forces between the linkages restrict the design space. The direction of the applied forces states the exact direction of the axis of notch hinges with respect to the *x*-axis [6]. As seen in Fig. 10, θ is the angle between the axis of the equivalent notch hinge and the *x*-axis. Angle θ is obtained using the direction of the applied forces to the rigid body model of the hinge (see the direction of the applied forces to the linkage 4 in Fig. 9). The thickness of the notch hinge, h, is smaller than the size of the connected linkages. In the current research, the diameter D is assigned to the two circular holes of the equivalent notch hinges, and angle $\theta = 16^\circ$ is used. The elastic hinge parameter, β can be obtained using the following equation [6]:

$$\beta = \frac{h}{D}. \tag{11}$$

It is recommended to keep the value of β in the range $0.01 < \beta < 0.5$ [6]. One can estimate β using flexural notch hinge reference plots (see Ref. [7] for a detailed explanation). According to the normalized reference stiffness plot in Ref. [7], the normalized rotation angle is defined as $\sigma_{\psi\psi}/(\psi E)$, where $\sigma_{\psi\psi}$ is the maximum allowable bending stress in the notch hinge, ψ is the rotation angle, and E is the Young's modulus of the hinge. Using the reference plot in Ref. [7], one can obtain β for small notch hinges (j_2, j_3, j_5, j_6, j_7, and j_8) and for large notch hinges (j_4 and j_9) to be $\beta = 0.294$ and $\beta = 0.0294$, respectively. In the current research, the parameters for small hinges are selected to be $h = 0.23$ mm and $D = 0.78$ mm, and for large hinges to be $h = 0.27$ mm and $D = 2.92$ mm.

Table 2
Material properties of the piezoelectric actuators used in the simulation [31].

Parameters	Symbol	Value	SI unit
Material	–	NCE51	–
Charge coefficient	d_{33}	443	10^{-12} C N^{-1}
Relative permitivity	$\frac{\epsilon^T}{\epsilon_0}$	1900	–
Elastic compliance	s^E	19	10^{-12} m^2 N^{-1}
Density	ρ_{piezo}	7850	kg m^{-3}
Dielectric loss factor	$\tan\delta$	150×10^{-4}	–
Mechanical quality factor	Q_m	80	–

3. Numerical study

Two numerical Finite Element models of the proposed flexural mechanism are examined in the present research: a rigid multibody model, and a flexible model. The rigid multibody model is used to find both the maximum relative rotation in the joints and the applied forces to the joints. The results of the rigid multibody model is used to find the flexure-based counterpart mechanism of the rigid mechanism. The flexible numerical model is used to evaluate the output displacement of the designed flexural mechanism. COMSOL Multiphysics 5.3a software package [32] is used to solve the coupled physics involved in the two numerical models, including the electrical and mechanical interfaces. In the numerical models, two piezoelectric stack actuators of type NAC2013-H30 manufactured by Noliac [31], are mounted in the *xy*-plane and along the *x*-axis (see Fig. 4). The actuators are connected to fixed hinges on one side. The other ends of the actuators are connected to linkages 1 and 7 (see Fig. 4). The material properties of the actuators are listed in Table 2. According to the manufacturer's data, the maximum allowable applied voltage to the piezoelectric actuators is 150 V [31]. In both numerical simulations, a sinusoidal voltage signal with a peak value of 75 V and a DC offset of 75 V is applied to the piezoelectric actuators to avoid a negative voltage. The applied voltage can be directly implemented in COMSOL Multiphysics to have a fully-coupled analysis. Therefore, the effect of the applied voltage to the actuators on the output motion of the suggested motion-converter mechanism can be investigated.

3.1. Rigid multibody analysis

The rigid multibody model of the proposed motion-converter mechanism is analyzed in COMSOL Multiphysics and is shown in Fig. 11(a) (see Fig. 3(a) for the schematic of the mechanism). The total displacement of the rigid multibody model is evaluated when

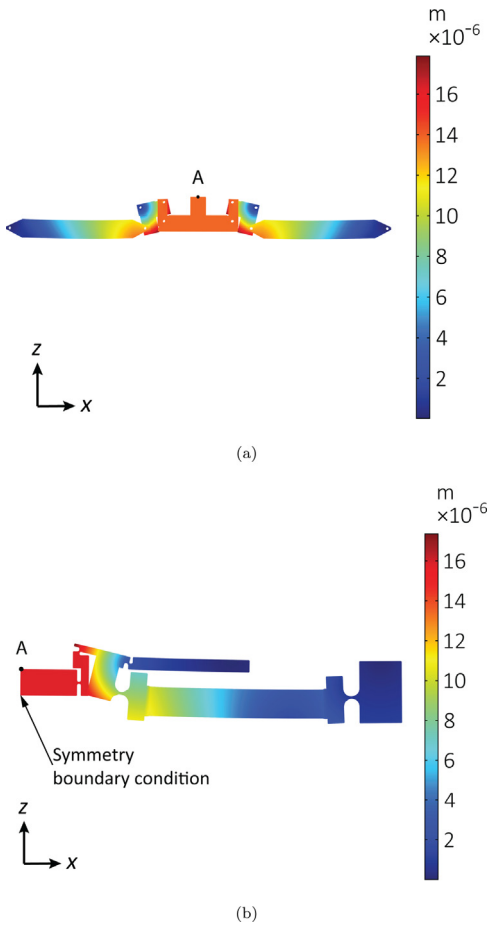

Fig. 11. Vertical displacement of the proposed motion-converter mechanism obtained from the numerical analysis; the displacements of the two models are shown at 20Hz with an applied voltage of 75 V AC and 75 V DC offset: (a) rigid multibody model; (b) flexural model.

Table 3
Relative rotation in the hinges of the rigid multibody model of the suggested motion-converter mechanism.

j_2	j_3	j_4	j_5	j_6	j_7	j_8	j_9
0.121°	−0.098°	0.049°	0.002°	0.098°	−0.121°	−0.002°	−0.049°

the maximum voltage signal of 75 V AC with a DC offset of 75 V is applied to the actuators. At a low frequency, for example at 20 Hz, the output displacement of the suggested mechanism is evaluated at point A using the FE analysis. A deformation factor of 150 is used in the figure to magnify the deformed geometry in the post-processing. The output displacement of the rigid multibody design at point A reaches 14 μm at 20 Hz. This value is approximately equal to the displacement of the piezoelectric actuators. Therefore, the amplification ratio of the suggested mechanism is approximately 1. The obtained output motion is relatively close to the required output motion of the suggested mechanism (see specifications in Section 1). As seen in the figure, a full geometry of the rigid multibody model of the motion-converter mechanism is analyzed in this research. The result of the rigid multibody analysis shows that the deformation of the two actuators are equal. The analysis of half of the geometry would be sufficient. Therefore, a half geometry of the flexural mechanism counterpart is used in the FE analysis in the following section to save computation time.

The applied forces to the hinge joints in the rigid multibody analysis and the resulting relative rotations are respectively shown in Fig. 12 and Table 3. The applied forces to hinges j_4 and j_9 reach a

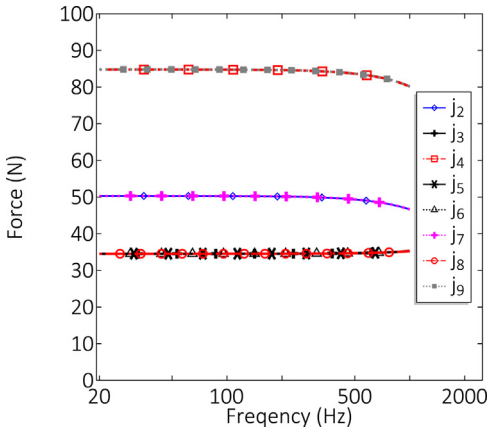

Fig. 12. Hinge force in the rigid multibody model of the suggested motion-converter mechanism.

maximum value of 85N. The forces in hinges j_4 and j_9 are applied by piezoelectric actuators. This maximum force in the hinges of the mechanism can be used as a design criterion.

The relative rotation of the hinge joints is listed in Table 3. The rotation in the hinges is constant over the frequency range of study in this research. The maximum rotation occurs in hinges j_2 and j_7. The reason is that these two hinges transfer the output motion of the actuators to the rigid multibody mechanism (see Fig. 4). The maximum rotation in this study is smaller than the maximum allowable rotation for small notch hinges (0.2° in this case [6]). This allows for the use of flexural notch hinges as the equivalent substitute [7].

The multibody body model in COMSOL Multiphysics 5.3a software contains 54,012 volume elements, and the number of degrees of freedom solved in the model is 74,660. The accuracy of the FE model is ensured using mesh refinement in the solver. Therefore, the relative error in the converged final result is investigated to find a sufficient accuracy which is not computationally expensive.

3.2. Flexural analysis

The rigid multibody model leads to finding the design parameters of its flexural counterpart. Hinge joints in the rigid multibody model are converted to their equivalent notch hinges. See Section 2.4.2 for the value of β for small and large notch hinges.

The maximum stress occurs in the hinges j_3, j_5, j_6, and j_8, with the value of 85 MPa at 1000 Hz. This maximum stress in both the rigid multibody model and the flexural mechanism is far below the yield stress of the structural Steel ($\sigma_{yield} = 300$ MPa).

The equivalent flexural mechanism is modeled in a 3D space using a symmetry boundary condition to avoid large computation time. It is modeled in 3D space instead of 2D space to take into account the analysis of the pre-stressing mechanism. The total displacement of the proposed flexural mechanism is shown in Fig. 11(b). As seen in the figure, the flexural model is in good agreement with its rigid counterpart. Similar to the rigid model, the output displacement of the flexural mechanism reaches 14 μm on the surface with the symmetry boundary condition. The use of flexural notch hinges at the two ends of the piezoelectric stack actuator ensures that axial loads are applied to the actuator.

The FE model of the flexural mechanism has 61,640 volume elements. The mesh includes 333,008 degrees of freedom. Similar to the rigid multibody model, the accuracy of the FE flexural model is ensured using mesh refinement in the solver.

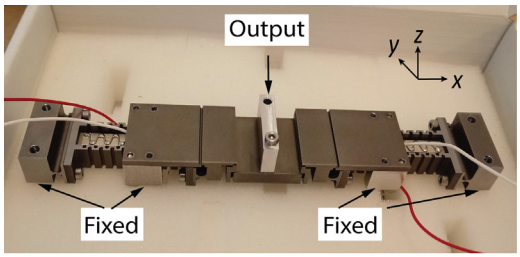

(a)

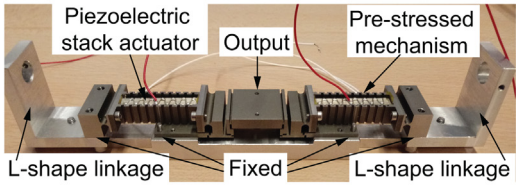

(b)

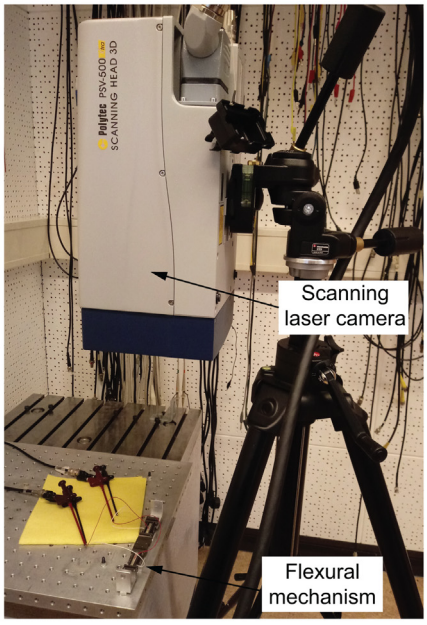

(c)

Fig. 13. The measurement setup: (a) the proposed flexural mechanism (top view) (b) the flexural mechanism (front view) that is connected to the auxiliary mechanism and is used in the measurement; (c) 3D scanning laser camera (model Polytec PSV-500).

4. Experiment

The measurement setup is shown in Fig. 13. The proposed flexural mechanism is built using structural steel and the wire eroding technique. As seen in Fig. 13(a), two piezoelectric stack actuators (model NAC2013-H30) are fitted in the designed pre-stressing flexural mechanism (see Section 2.3). Fig. 13(a) shows the constructed flexural mechanism that is actuated by two piezoelectric stack actuators. Fig. 13(b) shows the complete flexural mechanism that is used in the measurements. Auxiliary mechanisms (L-shape linkages shown in Fig. 13(b)) are used in the measurements to connect the flexural mechanism to the fixed world using fixture screws. A high voltage amplifier manufactured by Falco Systems (model WMA-300 [33]) is used to drive the piezoelectric actuators. Fig. 13(c) shows a 3D scanning laser camera vibrometer (model Polytec PSV-500 [34]) that is used to measure the output displacement of the flexural mechanism. Using the laser vibrometer camera, the output displacement of the motion-converter mechanism is measured in the direction of the *x*-, the *y*-, and the *z*-axis to ensure a pure translation motion in the output. The measurement can verify the pure translational motion in the direction of the *z*-axis as the output displacement of the flexure-based mechanism.

5. Results and discussions

To validate the performance of the designed mechanism, the results of the numerical simulation are compared with those obtained from the manufactured mechanism. To ensure that the connected amplifier is not overloaded during the measurement, especially at higher frequencies around 1000 Hz, the applied voltage to the piezoelectric actuators is kept as low as 9.75 V AC with a 10.8 V DC offset. A similar applied voltage is used in the numerical simulation to have a fair comparison.

5.1. Pre-stressing mechanism

Fig. 14 shows the displacement of a single pre-stressed piezoelectric mechanism at 20 Hz that is obtained from the numerical model. As seen in Fig. 14(a), one end of the pre-stressing mechanism is connected to a flexural notch hinge. To resemble a fixed hinge joint used in the rigid multibody counterpart (see Fig. 11(a)), the flexural notch hinge is connected to the fixed world through a fixed block. Fig. 14(b) shows that the other end of the pre-stressed piezoelectric mechanism is free to move.

Using the laser vibrometer scanning camera, the displacement of the free end of the pre-stressing mechanism in the direction of the *x*-axis is measured. During the measurement, the operating frequency changes from 20 Hz to 1000 Hz. Fig. 15 shows that the experimental and the numerical results are in good agreement. As seen in the figure, both numerical and experimental studies predict the resonance of the single pre-stressing mechanism at approximately 174 Hz. The vibration mode of the mechanism at the first resonance frequency is shown in the figure. Due to using an underestimated damping factor in the numerical model, a sharper resonance peak is seen in the numerical results when compared with those obtained from the measurements. This comparison between the numerical analysis and experimental study shows that the FE model is able to simulate the pre-stressed piezoelectric mechanism. The vibration mode in this figure is constrained in the complete flexural mechanism design, and therefore, does not occur. However, the FE model that is developed in this section can be useful in designing the complete FE model of the flexural mechanism in the following section.

5.2. Flexural mechanism

It was mentioned in Section 3.2 that a symmetry boundary condition was used in the FE analysis to avoid a computationally expensive 3D analysis in COSMOL Multiphysics. The first four mode shapes of the 3D symmetric model are predicted by the FEM and are shown in Fig. 16. As seen in the figure, all four mode shapes of the flexural mechanism occur at frequencies above 1000 Hz. Therefore, no resonance is seen in the frequency range of interest in this paper. This fulfills the requirement of having a rigid pistonic motion at the frequencies below 1000 Hz. According to the figure, the second mode shape of the motion-converter mechanism is a rotational mode around the *x*-axis which occurs above 2000 Hz. This resonance peak is not present in the frequency range of interest in the current paper (below 1000 Hz). Since this high order resonance peak is far from the fundamental resonance (see Fig. 16(a)), it can be concluded that no complex complementary control analysis

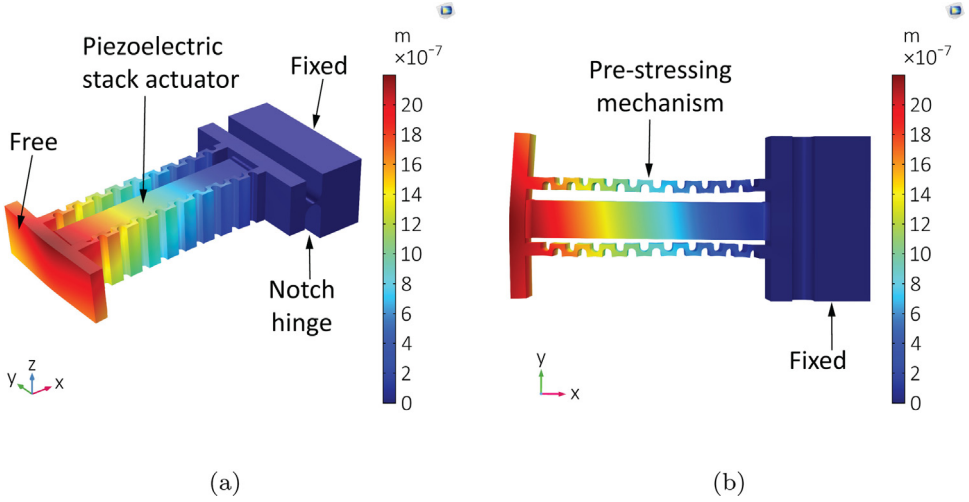

Fig. 14. Numerical result showing the displacement of a single pre-stressed piezoelectric mechanism with one end fixed and one end free at 20Hz at an applied voltage of 9.75 V AC with a DC offset of 10.8 V: (a) isometric view; (b) top view.

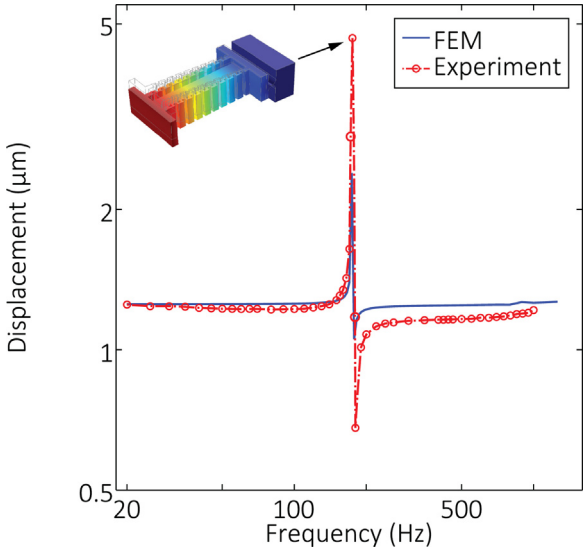

Fig. 15. A comparison between the experimental and the numerical FEM results showing the displacement of the free end of the pre-stressing mechanism in the direction of the *x*-axis, when the applied voltage is 9.75 V AC with a DC offset of 10.8 V.

is needed in further research to improve the accuracy of the output motion. It has to be noted that for the application in the thin acoustic source, the output motion of the complete coupled system, including the proposed actuation mechanism, has been also measured. The measurement result shows that there is no resonance peak associated with the proposed flexural mechanism in the piston-mode vibration of the acoustic source and up to the fundamental resonance of the complete system. This shows that the proposed flexural mechanism is suitable for the application in the thin acoustic source operating at low frequencies below 500 Hz.

The output displacement of the proposed flexural mechanism is measured using the test setup shown in Fig. 13. Fig. 17 shows a comparison between the numerical and the measurement results. It has to be noted that the measured output displacement of the proposed motion-converter mechanism shown in Fig. 17 is provided in the frequency range below 1000 Hz. During the measurement and at a specific frequency, a sinusoidal voltage with a peak value of 9.75 V and a DC offset of 10.8 V is applied to the two piezoelectric actuators, and the output displacement is measured. The measurement is repeated for several frequencies in the range between 20 Hz and 1000 Hz, while keeping the applied voltage constant. The outcome of this measurement is shown in Fig. 17. As seen in the figure, both the numerical and the experimental studies show that in a wide range of frequencies below 500 Hz, the output displacement of the flexural mechanism increases only slightly. This low frequency range is the main focus of this research in which the output motion of the flexural motion-converter mechanism increases relatively slowly. Above 500 Hz, the output displacement increases gradually as the frequency is closer to the fundamental resonance of the mechanism. The figure shows that the numerical and the experimental results are in very good agreement and the relative error is less than 15%. Therefore, the measurement validates the numerical FE model of the suggested flexure-based mechanism. The error, which is not larger than 15% in the frequency range of interest in this paper, is due to the applied voltage to the actuators. A detailed reasoning for this is addressed by a parametric study shown in Fig. 19 later in this section.

A Bode diagram of the applied force to the actuators is shown in Fig. 18, when the applied voltage to the actuators is the maximum allowable value (75VAC with an offset of 75 V). The evaluated applied force to the actuators is relatively constant in the low frequency range below 500 Hz. The FE model of the suggested flexural mechanism shows an applied force of approximately 95 N to the actuators. This obtained force is in accordance with the specifications in Section 1 and the obtained result in Section 3.1.

A parametric study reveals the accuracy of the numerical simulation at various applied voltages. The parametric study in Fig. 19 is useful to gain an insight on the cause of the error shown earlier in Fig. 17. In the parametric study, the relation between the output of the integrated motion-converter mechanism (output displacement) and the input of the mechanism (the input applied voltage to the actuators) is investigated. In the parametric study, the peak value of the applied AC voltage is increased from 1 V to 75 V, while the frequency remains constant. The DC offset in the applied voltage remains at 75 V in both the numerical and the experimental studies. To avoid overloading during the measurement of the connected amplifier, the experimental study is performed at low frequencies. If the connected amplifier had higher current overloading limit, the parametric study could have been measured at frequencies higher than 25 Hz. It is common in the industry to measure the displacement of the piezoelectric actuators with respect to the applied voltage at low frequencies to have a quasi-static operating condition [31]. In the current study, the lowest operating

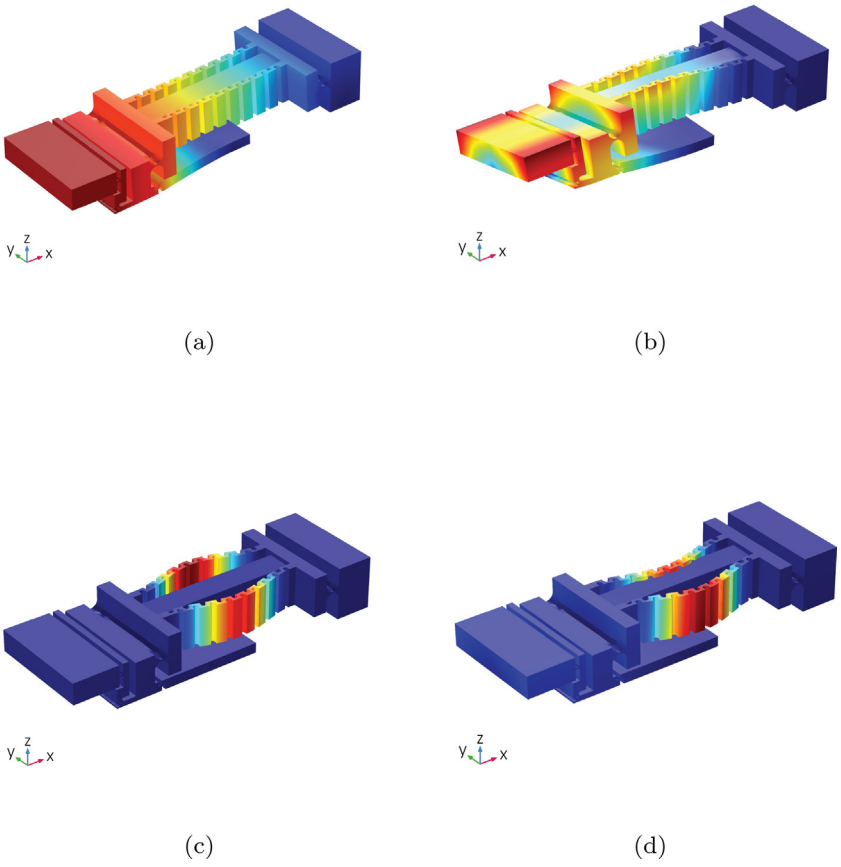

Fig. 16. Mode shapes of the complete proposed flexural mechanism simulated using COMSOL. Due to symmetry, only half of the mechanism is numerically modeled: (a) mode 1 at 1041 Hz; (b) mode 2 at 2321 Hz; (c) mode 3 at 3195 Hz; (d) mode 4 at 3215 Hz.

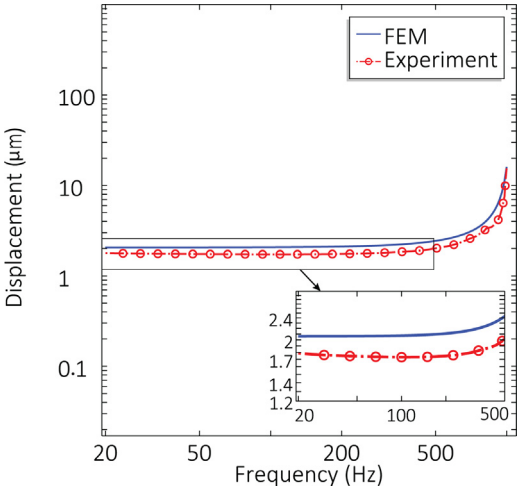

Fig. 17. A comparison between the experimental and the numerical FEM results showing the output displacement of the proposed flexural mechanism in the direction of the *z*-axis. The applied voltage to the piezoelectric actuators is 9.75 V AC with a DC offset of 10.8 V.

frequency of the piezoelectric actuators is limited to 10 Hz. At this low frequency, the presence of disturbance in the delivered input current to the piezoelectric actuators by the connected amplifier is inevitable. This disturbance limits the minimum operating frequency of the actuators in the experimental study. Therefore, the parametric study on the effect of the applied voltage to the actuators (between 1 V and 75 V) is limited to the operating frequencies between 10 Hz and 25 Hz. The measurement is repeated for the two low frequencies of 10 Hz and 25 Hz to investigate the effect of a change in the frequency on the result of the parametric study. The numerical simulation is performed at the same frequencies. A comparison between the numerical and the experimental results is shown in Fig. 19. As seen in the figure, the results of the FE analysis at the two frequencies are almost identical. However, in practice, due to the presence of tolerance in both the piezoelectric stack actuators and the flexural mechanism, which is imposed during the construction process, the measured displacement slightly deviates at the two frequencies. Flexural mechanisms have low hysteresis. However, some hysteresis can be caused by the connected piezoelectric actuators. In addition, flexural mechanisms that consist of multiple assembled parts can have hysteresis (micro-slips). Due to monolithic design of the proposed actuation mechanism, hysteresis is not present in the core part. However, it can be present as micro-slip in the connection surfaces of the fixed parts and the pre-stressing mechanism. The deviation in Fig. 19 can be a result of hysteresis in the connected piezoelectric stack actuators [31]. The hysteresis effect for the piezoelectric actuator that is used in the motion-converter mechanism is investigated in Ref. [35]. The hysteresis effect is determined to be approximately 1.5% of the free stroke of the piezoelectric actuator. According to the manufacturer, the hysteresis effect can be as high as 19%, which is a direct result of aging in the actuator [31]. Fig. 19 shows that the variation between the measured displacement and the numerical one is minimal at the peak applied voltage of approximately 55 V. For applied peak voltages lower than 55 V, the numerical analysis overestimates the output displacement of the flexural mechanism. On the other hand, at voltages higher than 55 V, the FE study underestimates this parameter. The deviation of 15% between the numerical and the experimental results, which was earlier shown in Fig. 17, can be explained

using the results of Fig. 19. The reason for this deviation is that the applied peak voltage in the measurement in Fig. 17 is 9.75 V. This low voltage in the measurement is used to avoid overloading of the connected amplifier at higher frequencies. According to the result of Fig. 19, due to the applied peak voltage of 9.75 V, which is below 55 V, the FE model predicts a displacement higher than the measurement does. If a connected amplifier with higher current limit is used, the applied voltage to the piezoelectric actuators can be increased to 55 V. At this voltage, the minimum deviation between the numerical and the measurement results in Fig. 17 can be achieved. This minimum deviation improves the accuracy of the proposed design. Figs. 17 and 19 reveal that the numerical model can accurately predict the mechanical behavior of the proposed flexural mechanism.

The accuracy of the symmetry boundary condition that is used in the numerical model is validated by measuring the output velocity of the flexural mechanism in the direction of the *x*- and the *y*-axis, relative to the velocity in the *z*-direction. To verify that the proposed motion-converter mechanism has a pure translation output motion, the parasitic motions in the direction of the *x*- and the *y*-axis is investigated using the 3D scanning laser camera vibrometer (model Polytec PSV-500). In the low frequency range below 500 Hz, the velocity of the proposed mechanism in the direction of the *x*- and the *y*-axis remains relatively small as an inclined line with a constant slope, especially in the logarithmic scale. At a low frequency below 500 Hz, for instance at 200 Hz, the lateral axes velocities in the direction of the *x*- and the *y*-axis are measured respectively at 0.124 $\mu m\,s^{-1}$ and 0.0129 $\mu m\,s^{-1}$, while the velocity in the direction of the *z*-axis is approximately 2236 $\mu m\,s^{-1}$. The velocity ratio between the lateral axes velocities and the velocity in the direction of the *z*-axis is very low. This velocity ratio is respectively 5.54×10^{-5} and 5.77×10^{-6} in the direction of the *x*- and the *y*-axis. These low velocity ratios remain relatively constant in the low frequencies below 500 Hz and hence the parasitic motion is negligible in the lateral axes in this low frequency range. The measurement results show that the output motion of the proposed flexural mechanism can be reasonably considered as a pure translation displacement in the direction of the *z*-axis. Therefore, considering a symmetry boundary condition in the FE model is a reasonable assumption.

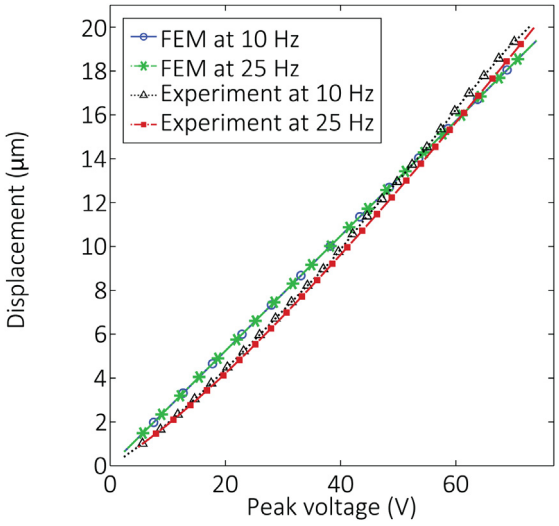

Fig. 19. A comparison between the experimental and the numerical FEM results showing the output displacement of the proposed flexural mechanism in the direction of the *z*-axis and as a function of the peak of the applied AC voltage. Studies are repeated for the two frequencies of 10 Hz and 25 Hz.

6. Summary and conclusions

In this paper, a thin flexural mechanism is proposed as a motion-converter. The proposed mechanism is useful in applications where the available space in the direction of the output motion is limited, and long piezoelectric stack actuators are needed to enable sufficient displacement. The dimension of the mechanism in the direction of the final motion is 10.5 mm, and the length of the core mechanism is approximately 77 mm. The proposed mechanism can translate the displacements of two piezoelectric stack actuators in the direction of the *x*-axis to a pure translation output motion in the direction of the *z*-axis. A desired design in this research does not have any resonance peaks at frequencies below 1000 Hz. The numerical and the experimental studies show that the proposed mechanism has a first resonance outside the frequency range of interest in this research. According to both studies, the

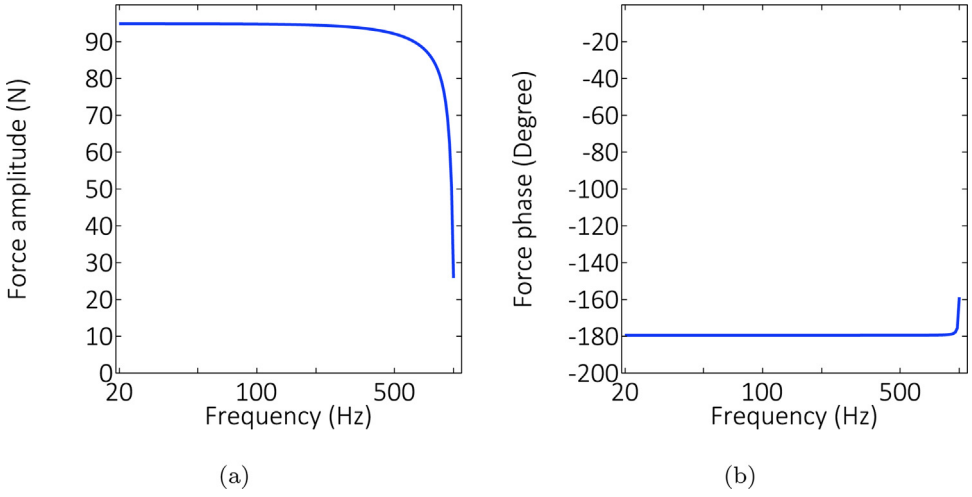

Fig. 18. Bode diagram of the applied force to the piezoelectric stack actuators in the motion-converter mechanism that is obtained from FE analysis, when the applied voltage to the actuators is a sinusoidal signal with an amplitude of 75 V and an offset of 75 V: (a) amplitude; (b) phase.

displacement of the proposed mechanism remains relatively constant in a wide range of frequencies below 500 Hz in this research. The numerical and the experimental results show that the output displacement of the flexural mechanism can be reasonably considered as a pure translational motion in the direction of the *z*-axis. The measured displacement of the proposed flexural mechanism in the output stage and in the direction of the *x* and the *y*-axis is negligible. The pure translational output motion is due to using two actuators in the symmetric design of the proposed mechanism. The two actuators eliminate the presence of any parasitic motion in other directions. The measurement results verify the accuracy of the numerical simulation with an error of less than 15%. A parametric study shows that the variation between numerical and experimental results is due to the existence of tolerance in both the piezoelectric stack actuators and the proposed flexural design which is imposed during the manufacturing process. Therefore, both numerical and experimental studies are in good agreement. According to the measurement results, depending on the applied peak voltage to the actuators and the operating frequency, the error between the FEM and the experimental results can vary but not more than 15%.

Authors' contributions

Farnaz Tajdari: Conceptualization, Methodology, Software, Validation, Formal analysis, Investigation, Writing – Original Draft.

Arthur P. Berkhoff: Supervision.

Mark Naves: Writing – Reviewing and Editing, Supervision.

Marijn Nijenhuis: Writing – Reviewing and Editing, Supervision.

André de Boer: Writing – Reviewing and Editing, Supervision.

Declaration of Competing Interest

The authors report no declarations of interest.

Acknowledgements

The authors gratefully acknowledge the European Commission for its support of the Marie Skłodowska Curie program through the ITN ANTARES project (GA 606817). The construction of the proposed design for experimental development is supported by Leo Tiemersma of the Faculty of Engineering Technology, University of Twente.

Appendix A. Supplementary data

Supplementary data associated with this article can be found, in the online version, at https://doi.org/10.1016/j.sna.2020.112198.

References

[1] X. Wang, C. Ehlers, M. Neitzel, Electro-mechanical dynamic analysis of the piezoelectric stack, Smart Mater. Struct. 5 (4) (1996) 492 http://stacks.iop.org/0964-1726/5/i=4/a=013.

[2] M. Mitrovic, G. Carman, F. Straub, Electromechanical characterization of piezoelectric stack actuators, Proc. SPIE 3668 (1999), http://dx.doi.org/10.1117/12.350689, 3668–3668–16.

[3] W. Zhu, G. Chen, X. Rui, Modeling of piezoelectric stack actuators considering bonding layers, J. Intell. Mater. Syst. Struct. 26 (17) (2015) 2418–2427, http://dx.doi.org/10.1177/1045389X15575083.

[4] S. Naikwad, R. Vandervelden, S. Hosseinnia, Self-sensing contact detection in piezo-stepper actuator, 2016 12th IEEE/ASME International Conference on Mechatronic and Embedded Systems and Applications (MESA) (2016) 1–6, http://dx.doi.org/10.1109/MESA.2016.7587186.

[5] F. Tajdari, A. Berkhoff, A. de Boer, Numerical modeling of a flexural displacement-converter mechanism to excite a flat acoustic source driven by piezoelectric stack actuators, in: Proceedings of the International Conference on Noise and Vibration Engineering ISMA 2018, KULeuven, Leuven, Belgium, 2018 https://research.utwente.nl/en/publications/numerical-modeling-of-a-flexural-displacement-converter-mechanism.

[6] S. Smith, Flexures, Elements of Elastic Mechanisms, CRC Press, University of North Carolina, USA, 2000, urlhttps://www.crcpress.com/Flexures-Elements-of-Elastic-Mechanisms/Smith/p/book/9789056992613https://www.crcpress.com/Flexures-Elements-of-Elastic-Mechanisms/Smith/p/book/9789056992613.

[7] H. Soemers, Design Principles for Precision Mechanisms, T-Pointprint University of Twente, The Netherlands, 2011 https://www.t-pointprint.nl/?page_id=218.

[8] J. Juuti, K. Kordás, R. Lonnakko, V. Moilanen, S. Leppävuori, Mechanically amplified large displacement piezoelectric actuators, Sens. Actuators A: Phys. 120 (1) (2005) 225–231, http://dx.doi.org/10.1016/j.sna.2004.11.016 http://www.sciencedirect.com/science/article/pii/S0924424704008337.

[9] M. Ling, J. Cao, M. Zeng, J. Lin, D. Inman, Enhanced mathematical modeling of the displacement amplification ratio for piezoelectric compliant mechanisms, Smart Mater. Struct. 25 (7) (2016) 075022 http://stacks.iop.org/0964-1726/25/i=7/a=075022.

[10] Y. Yong, S. Aphale, S. Moheimani, Design, identification, and control of a flexure-basedxystage for fast nanoscale positioning, IEEE Trans. Nanotechnol. 8 (1) (2009) 46–54, http://dx.doi.org/10.1109/TNANO.2008.2005829.

[11] Y. Li, Q. Xu, A novel piezoactuated xy stage with parallel, decoupled, and stacked flexure structure for micro-/nanopositioning, IEEE Trans. Ind. Electron. 58 (8) (2011) 3601–3615, http://dx.doi.org/10.1109/TIE.2010.2084972.

[12] Y. Li, Q. Xu, A totally decoupled piezo-driven xyz flexure parallel micropositioning stage for micro/nanomanipulation, IEEE Trans. Autom. Sci. Eng. 8 (2) (2011) 265–279, http://dx.doi.org/10.1109/TASE.2010.2077675.

[13] Y. Yong, Preloading piezoelectric stack actuators in high-speed nanopositioning systems, Front. Mech. Eng. 2 (2016) 8, http://dx.doi.org/10.3389/fmech.2016.00008.

[14] T. Lee, I. Chopra, Design of a Bidirectional Piezoelectric Actuator for Blade Trailing-Edge Flap, 2001, http://dx.doi.org/10.1117/12.436552.

[15] J. Feenstra, J. Granstrom, H. Sodano, Energy harvesting through a backpack employing a mechanically amplified piezoelectric stack, Mech. Syst. Signal Process. 22 (3) (2008) 721–734, http://dx.doi.org/10.1016/j.ymssp.2007.09.015 http://www.sciencedirect.com/science/article/pii/S0888327007001951.

[16] Y. Wang, W. Chen, P. Guzman, Piezoelectric stack energy harvesting with a force amplification frame: modeling and experiment, J. Intell. Mater. Syst. Struct. 27 (17) (2016) 2324–2332, http://dx.doi.org/10.1177/1045389X16629568.

[17] J. Kim, S. Kim, Y. Kwak, Development and optimization of 3-d bridge-type hinge mechanisms, Sens. Actuators A: Phys. 116 (3) (2004) 530–538, http://dx.doi.org/10.1016/j.sna.2004.05.027 http://www.sciencedirect.com/science/article/pii/S0924424704003486.

[18] J. Liu, W. O'Connor, E. Ahearne, G. Byrne, Electromechanical modelling for piezoelectric flextensional actuators, Smart Mater. Struct. 23 (2) (2014) 025005, http://dx.doi.org/10.1088/0964-1726/23/2/025005 http://stacks.iop.org/0964-1726/23/i=2/a=025005.

[19] M. Muraoka, S. Sanada, Displacement amplifier for piezoelectric actuator based on honeycomb link mechanism, Sens. Actuators A: Phys. 157 (1) (2010) 84–90, http://dx.doi.org/10.1016/j.sna.2009.10.024 http://www.sciencedirect.com/science/article/pii/S0924424709004622.

[20] J. Guo, S. Chee, T. Yano, T. Higuchi, Micro-vibration stage using piezo actuators, Sens. Actuators A: Phys. 194 (2013) 119–127, http://dx.doi.org/10.1016/j.sna.2013.01.025 http://www.sciencedirect.com/science/article/pii/S0924424713000381.

[21] T. Yeom, T. Simon, M. Zhang, M. North, T. Cui, High frequency, large displacement, and low power consumption piezoelectric translational actuator based on an oval loop shell, Sens. Actuators A: Phys. 176 (2012) 99–109, http://dx.doi.org/10.1016/j.sna.2012.01.001 http://www.sciencedirect.com/science/article/pii/S0924424712000258.

[22] J. Chen, C. Zhang, M. Xu, Y. Zi, X. Zhang, Rhombic micro-displacement amplifier for piezoelectric actuator and its linear and hybrid model, Mech. Syst. Signal Process. 50–51 (2015) 580–593, http://dx.doi.org/10.1016/j.ymssp.2014.05.047 http://www.sciencedirect.com/science/article/pii/S0888327014002234.

[23] F. Claeyssen, R. Le Letty, F. Barillot, O. Sosnicki, Amplified piezoelectric actuators: static & dynamic applications, Ferroelectrics 351 (1) (2007) 3–14, http://dx.doi.org/10.1080/00150190701351865.

[24] R. Lucinskis, C. Mangeot, Dynamic Characterization of an Amplified Piezoelectric Actuator, 2016 http://www.noliac.com/fileadmin/user_upload/images/Tutorials/Publications/Noliac_publications/Actuator_2016_Dynamic_characterization_of_an_amplified_piezoelectric_actuator.pdf.

[25] Electrical Discharge Machining, https://en.wikipedia.org/wiki/Electrical_discharge_machining (Online; accessed 11.06.19).

[26] IEEE Standard on Piezoelectricity, https://doi.org/10.1109/IEEESTD.1988.79638.

[27] A. Ballato, Modeling piezoelectric and piezomagnetic devices and structures via equivalent networks, IEEE Trans. Ultrason. Ferroelectr. Freq. Control 48 (5) (2001) 1189–1240, http://dx.doi.org/10.1109/58.949732.

[28] Y. Zhang, T. Lu, Y. Peng, Three-port equivalent circuit of multi-layer piezoelectric stack, Sens. Actuators A: Phys. 236 (2015) 92–97, http://dx.doi.org/10.1016/j.sna.2015.10.033 http://www.sciencedirect.com/science/article/pii/S0924424715301941.

[29] Noliac, http://www.noliac.com/tutorials/faq/ (Online; accessed 20.05.19).

[30] Cedrat Technologies, https://www.cedrat-technologies.com/en/products/actuators/parallel-pre-stressed-actuators.html (Online; accessed 20.05.19).
[31] Specifications NAC2013-H30, noliac, http://www.noliac.com/products/actuators/plate-stacks/show/nac2013-hxx/ (Online; accessed 16.05.19).
[32] COMSOL, Multiphysics 5.3a, Release Notes, https://cdn.comsol.com/documentation/5.3.1.348/COMSOL_ReleaseNotes.pdf (Online; accessed 20.05.19).
[33] Falco Systems, WMA-300 High Speed High Voltage Amplifier, http://www.falco-systems.com/High_voltage_amplifier_WMA-300.html (Online; accessed 16.05.19).
[34] PSV-500-3D, Scanning Vibrometer, Datasheet, https://www.polytec.com/fileadmin/d/Vibrometrie/OM_DS_PSV-500-3D_E_42447.pdf (Online; accessed 21.05.19).
[35] F. Tajdari, A. Berkhoff, A. de Boer, Numerical modeling of electrical-mechanical-acoustical behavior of a lumped acoustic source driven by a piezoelectric stack actuator, in: Proceedings of the International Conference on Noise and Vibration Engineering ISMA 2016, KULeuven, Leuven, Belgium, 2016 https://research.utwente.nl/en/publications/numerical-modeling-of-electrical-mechanical-acoustical-behavior-o.

Biography

Farnaz Tajdari received her Bachelor's degree in Mechanical Engineering in 2012 and her Master's degrees in Energy Systems Engineering in 2014 from K.N. Toosi University of Technology, Iran. She started her PhD in Mechanical Engineering at University of Twente, the Netherlands in 2015. She was a Marie Curie fellow and her PhD research was funded by European Commission through the ITN ANTARES project (GA 606817). She received her PhD degree in 2019.